PAPER

Enhanced fluorescent effect of graphitic C₃N₄@ZIF-8 nanocomposite contribute to its improved sensing capabilities†

Wei Chen, [ID] Shu Kong, Jian Wang, Liping Du, Wen Cai and Chunsheng Wu [ID]*

A novel graphitic carbon nitride (g-C₃N₄)@ZIF-8 nanocomposite was synthesized by a facile approach and applied as a fluorescent sensor. The fluorescent quenching and enhancing effect of g-C₃N₄@ZIF-8 nanocomposite was explored for potential applications in sensing metal ions and solvents based on photoluminescence (PL) measurements. Compared with g-C₃N₄ nanosheets alone, the combined g-C₃N₄@ZIF-8 nanostructure greatly improved the sensitivity for the detection of metal ions due to the special fluorescent quenching effect. In particular, the sensitivities of the detection of Cu^{2+} and Ag^+ improve from 29.1 to 11.2 ppm and from 40 to 16.5 ppm, respectively, which were significantly improved compared to that of g-C₃N₄ nanosheets alone. The sensitivity could increase about 100% and 250% for Cu^{2+} and Ag^+ by the g-C₃N₄@ZIF-8. The limit of detection (LOD) for Cu^{2+} and Ag^+ by g-C₃N₄@ZIF-8 was 11.2 ppm and 13.2 ppm, respectively. Both g-C₃N₄ nanosheets and g-C₃N₄@ZIF-8 nanocomposite can be used for distinguishing Fe^{2+} and Fe^{3+} in solutions. The LOD of Fe^{2+} by g-C₃N₄@ZIF-8 was as low as 65.4 ppm. On the other hand, the relative increased luminescence of g-C₃N₄@ZIF-8 to the g-C₃N₄ in tetrahydrofuran (THF) was selective, which was successfully applied for detecting this specific solvent. An excellent linear relationship (0–1.0 v/v of THF/water) between the THF fraction and PL intensities was obtained. These results demonstrate that the g-C₃N₄@ZIF-8 nanocomposite provide a convenient and novel approach for the enhance fluorescence detection of metal ions and distinguishing of specific solvents.

1   Introduction

Heavy metal ions and their derivatives are of great current interest owing to their severe adverse impact on the environment and human health.[1] For example, copper is an essential trace element for the living organisms, but an excessive copper is toxic when it accumulated in living organism.[2] Similar to copper ion, silver ion can accumulate in the living organism and cause severe physiological problem.[3] Through various absorption channels such as soil, reservoir water, food, these heavy metal ions can gather in developing brains, or binding to protein/peptide, leading to debilitating diseases.[4] As a result, a variety of methods have been developed for detecting the harmful heavy metal ions, for example, coupled plasma mass spectroscopy,[5] atomic absorption spectroscopy,[6] Raman spectroscopy,[7] electrochemical method,[8] and fluorescent methods.[1] Among these methods, fluorescent method is facial and highly sensitive.[9] Organic dyes and semiconductor quantum dots are

the most commonly used fluorescent probes.[1] However, these materials suffer from some intrinsic detects such as easy oxidation, photobleaching, high toxicity and cost, which hampered their practical applications greatly.[10] Therefore, it is highly desirable to develop novel materials to address these issues, which are suitable to be used as sensitive elements for the detection of metal ions.

Metal–organic frameworks (MOFs), self-assembled by the coordination of metal ion/cluster with organic linkers, is a new porous material.[11] The structural rigidity, high porosity, and turntable component support its potential applications in a variety of fields, such as gas separation and storage,[12] catalysis,[13] sensing,[14] and biomedical applications.[15] ZIF-8 is often composited by a zinc ion center and 2-methylimidazole (Hmim) ligand, which belongs to the superfamily of MOFs and possess a sodalite (SOD)-type structure.[16] Pyridyl nitrogen sites have been reported to be able to selectively bind to metal ions and used as metal ion sensor.[17] With similar structure, imidazole-based conjugated polymer has also been reported to be used as a metal ion sensor.[18] Since the imidazole nitrogen has specific affinity to metal ions, ZIF-8 can be used for detecting the metal ions.[19] However, the fluorescence of ZIF-8 is low and thus limits its selectivity and detection sensitivity. Thus, ZIF-8 encapsulated AlQ₃ (tris(8-hydroxyquinoline)-aluminium), FITC

Institute of Medical Engineering, Department of Biophysics, School of Basic Medical Sciences, Health Science Center, Xi'an Jiaotong University, Xi'an 710061, China. E-mail: wuchunsheng@xjtu.edu.cn; Fax: +86-29-82657763; Tel: +86-29-82657763

(fluorescein isothiocyanate) and Eu(III)-complex-functionalized Fe_3O_4, and Zn_2GeO_4:Mn^{2+} nanorods were reported as a luminescent ions sensor.[20–22]

Recently, graphitic carbon nitride (g-C_3N_4) has attracted much attention due to its decisive advantages such as easy preparation, high thermal stability, high visible photocatalysis activity, and high water splitting activity.[23–25] Fluorescent g-C_3N_4 quantum dots used for detecting heavy metal ions have been reported very recently.[26–29] The selectivity and sensitivity of g-C_3N_4 for detecting copper ions are reasonable because the photoinduced electron transfer (PET) between the CB of g-C_3N_4 to the complexed Cu^{2+} leading to the fluorescent quenching.[26] Additionally, g-C_3N_4 decorated ball-like Co_3O_4 composite exhibited 1.6 times higher sensitivity than that of pure Co_3O_4.[30] The g-C_3N_4/Bi_2MoO_6 composite which displayed nearly 3-fold and 6-fold enhanced photocurrent intensity than pure g-C_3N_4 and Bi_2MoO_6, could be applied in copper ion sensor with a linear range from 3 nM to 40 μM by a photoelectrochemical method.[31] The C_3N_4-tyrosinase hybrid was a sensitive fluorescent probe for the detection of dopamine with detection limit as low as 3×10^{-8} mol L^{-1}.[32] Many carbon nitride nanohybrid, including C_3N_4/metal oxide nanoparticles, metal nanoparticles, metal–organic frameworks, graphene have been applied in the sensor application.[33–38]

It is thus tempted to combine the advantages of g-C_3N_4 and ZIF-8 to develop novel materials that are suitable for sensing metal ions. Herein, a facile method was developed for the preparation of g-C_3N_4@ZIF-8 nanocomposite that is suitable to be used as sensitive elements for the detection of metal ions and solvents. The morphology and structure of g-C_3N_4@ZIF-8 nanocomposite was characterized. Photoluminescence (PL) measurements were carried out to test the performance of g-C_3N_4@ZIF-8 nanocomposite for sensing metal ions. The fluorescent quenching effect can not only be found during sensing copper and silver ions, but also be observed during sensing Fe^{2+}. On the contrary, the Fe^{3+} has little fluorescent quenching effect. The comparative phenomenon on Fe^{2+} and Fe^{3+} fluorescent quenching effect could be used for distinguishing the Fe^{2+} and Fe^{3+}. In addition, compare to other solvents, tetrahydrofuran (THF) has the most enhancive fluorescence for g-C_3N_4@ZIF-8, which could be potentially applied for distinguishing this THF from other solvents.

2   Materials and methods

2.1   Materials

Melamine, $Zn(NO_3)_2 \cdot 6H_2O$, $HgCl_2$, $CaCl_2$, NaCl, $FeCl_2$, $FeCl_3$, KCl, $MnCl_2 \cdot 4H_2O$, $Li(CH_3COO)_2$, $SnCl_2$, $CoCl_2 \cdot 6H_2O$, $AgNO_3$, $CuCl_2$, $Ni(NO_3)_2 \cdot 6H_2O$ were ordered from Sinopharm Chemical Reagent Co., Ltd. Tetrahydrofuran (THF), 2-methylimidazole (Hmim), dimethylformamide (DMF), ethanol, methanol, and acetone were purchased from Sigma Aldrich. All the other chemicals were analytical pure grade or better quality. Deionized water (18.2 MΩ cm^{-1}) produced by a Milli-Q system (Bedford, MA) was used throughout.

2.2   Synthesis of the g-C_3N_4 nanosheet

The g-C_3N_4 nanosheet was synthesized according to previous report.[39] For the first, bulk C_3N_4 was firstly synthesized by pyrolysis of melamine. Typically, 5 g melamine was heated to 550 °C with a ramp rate of 3°C min^{-1} and maintained at the final temperature for 4 h in the air environment. For the next, the resultant yellow powder was milled for thermal treatment. The thermal treatment was conducted in an open ceramic container with a heating rate of 5 °C min^{-1} to 500 °C and maintained for 2 h. Through the process, the yellow powder turned into a light-yellow product.

2.3   Synthesis of the g-C_3N_4@ZIF-8

Graphitic C_3N_4@ZIF-8 was synthesis by an *in situ* method. Briefly, 10 mg of g-C_3N_4 was firstly dissolved into a 5 mL of 75 mM Hmim methanol solution and stirred for 10 min. Then, 5 mL of 150 mM $Zn(NO_3)_2 \cdot 6H_2O$ methanol solution was added. For the next, the solution was left undisturbed for 2 h. The finally product was collected by the centrifugation method and washed with methanol for 3 times.

2.4   PL measurements

For sensing various metal ions, 0.2 mL of 1 mM g-C_3N_4@ZIF-8 DMF solution was added to 6 mL of DMF to form a homogeneous solution. Certain volumes of 1 mM DMF solution with metal ions were added to the g-C_3N_4@ZIF-8 solution. The excitation wavelength was 330 nm and the emission peak were 450 nm. Since silver ions can be reduced by DMF,[40] silver ion test was conducted in aqueous solution.

For sensing properties with respect to various solvents, 0.2 mL g-C_3N_4@ZIF-8 solution was added to 6 mL solvent (DMF, distilled water, acetone, methanol, ethanol, THF). After shaking 2 min, 3 mL of the solution was used for PL measurements.

2.5   Characterization

X-ray diffraction (XRD) patterns of the samples were recorded on a D2 PHASER (BRUKER) diffractometer with Cu Kα irradiation, 30 kV, 10 mA. The structure and morphology of the samples were determined by scanning electron microscopy (SEM) and transmission electron microscopy (TEM) performed on PHILIPS XL30 and PHILIPS Tecnai 12, respectively. Fourier transform infrared spectroscopy (Spectrum 100, PerkinElmer) spectrum of samples were recorded using a KBr disk in the range of 4000 to 400 cm^{-1}. Nitrogen physisorption isotherms were measured at 77 K on automatic Nova Station A. The UV-visible spectrum was performed on Agilent Cary 4000. The PL spectroscopy of the samples was carried on Hitachi F 4600.

3   Results and discussion

3.1   Characterization of g-C_3N_4@ZIF-8

Enable to test the PL spectrum, the stability of the nanoparticles is of great importance. Therefore, the dispersion of g-

C_3N_4@ZIF-8 nanocomposite and g-C_3N_4 nanosheet in DMF solution was investigated at different times. The result indicates that the g-C_3N_4@ZIF-8 nanocomposite solution was more homogeneous and stable than that of bulk g-C_3N_4 solution (Fig. 1), which indicating the PL intensity change was only induced by the metal ions but not the nanoparticles sedimentation. This suggested a good stability of g-C_3N_4@ZIF-8 nanocomposite was suitable for PL spectrum measurements.

The morphologies of g-C_3N_4 nanosheet and g-C_3N_4@ZIF-8 were observed by SEM and TEM, respectively. As shown in Fig. 2, the results indicate the g-C_3N_4 dispersed well and was the analogue of wrinkled graphene. After *in situ* decorated with ZIF-8, small nanoparticles assembled on the g-C_3N_4 nanosheet, leaving fewer margins. This ensured that the metal ions or solvents must cross the pores of ZIF-8 to interact with g-C_3N_4. The high resolution TEM images indicated that all nanoparticles assembled on the nanosheet with average diameter of 50 nm. In addition, N_2 absorption and desorption isotherms of the g-C_3N_4@ZIF-8 (Fig. S1†) further confirm its surface area and the pore structure.

The structure of the nanocomposite was confirmed by XRD pattern. As shown in Fig. 3a, a peak of 7.0° was the characteristic of ZIF-8. The sharp peak at 27.7° corresponded to the nanosheet of g-C_3N_4.[39] The further FTIR spectrum confirmed the component (Fig. 3b). The sharp peak at around 810 cm^{-1} was originated from heptazine ring system. The peaks range from 900 to 1800 cm^{-1} were associated to C–N–C or C–NH–C units.[39] The peak at 421 cm^{-1} was attributed to Zn–N stretching. And peaks 1350–1500 cm^{-1} were attributed to the entire ring stretching of imidazole.[41] The UV-visible spectra results indicated that after decorated with ZIF-8, the absorption edge and peak of g-C_3N_4 did not shift (Fig. 3c). The strong peak at 319 nm was the characteristic peak of g-C_3N_4.[26] Besides this peak, g-C_3N_4 also had two peaks at 370 nm and 380 nm, respectively. When excited at 320 nm, the emission peak appeared at 450 nm, which indicated the nanocomposite was fluorescent. To check whether the g-C_3N_4@ZIF-8 was an excitation-independent PL material, different excitation wavelength was applied. As showed in the Fig. 3d, when the excitation wavelength changed from 310 nm to 370 nm, the PL spectra did not shift, and a peak around 450 nm was invariable.

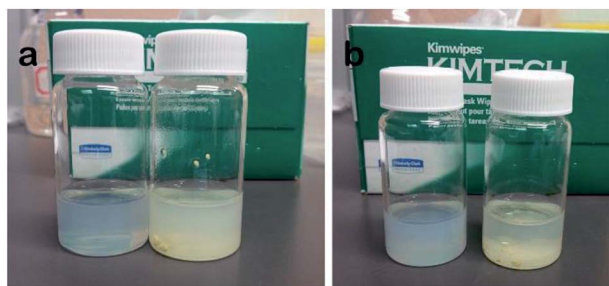Fig. 2 (a) SEM image and (b) TEM image of g-C_3N_4 nanosheets; (c) SEM image and (d) and (e) TEM images of g-C_3N_4@ZIF-8 nanostructures.

3.2 Detection of metal ions

Screening experiments with different metal ions (66 ppm) were carried out by investigating the changes in PL intensity of the g-C_3N_4@ZIF-8. As showed in Fig. 4, the PL intensities of g-C_3N_4@ZIF-8 were greatly decreased by Fe^{2+}, Cu^{2+} and Ag^+, while the other ions presented less or no effect. This indicated that g-C_3N_4@ZIF-8 was sensitive to the specific ions and can be used as sensitive elements for the fluorescent detection of metal ions. The sensitivity of g-C_3N_4@ZIF-8 for Fe^{2+}, Cu^{2+} and Ag^+ may be due to the higher binding affinity of these ions to N of the ZIF-8 and g-C_3N_4.[17–19,42,43] Due to the high porosity of ZIF-8, a large

Fig. 1 Dispersion of g-C_3N_4@ZIF-8 nanostructure (left) and bulk g-C_3N_4 (right) in DMF solution at different times: (a) 0 min, (b) 10 min.

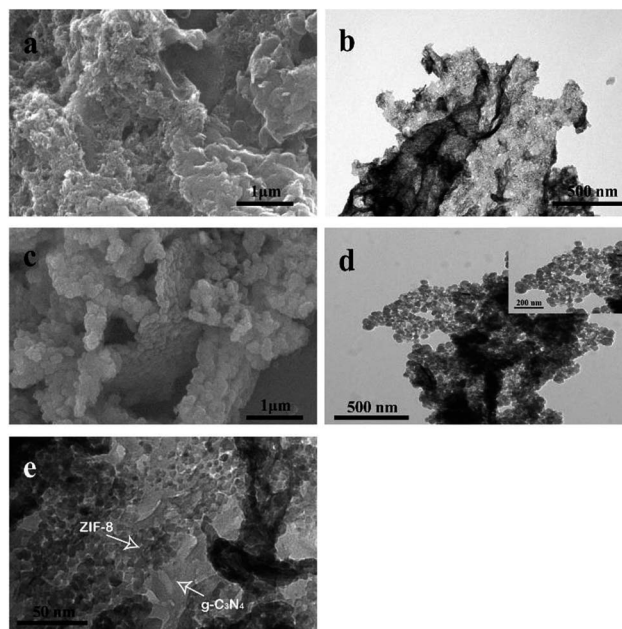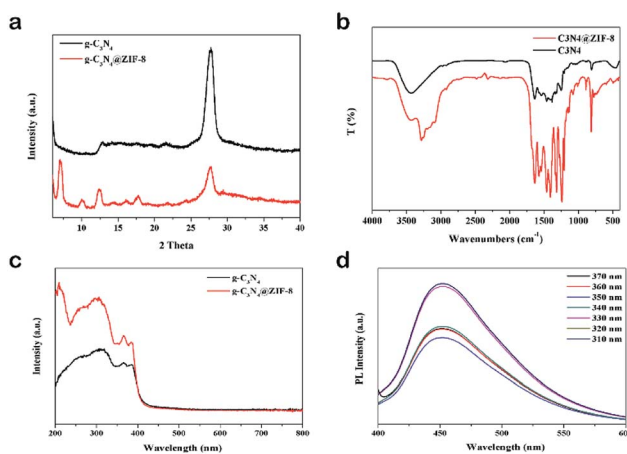Fig. 3 (a) XRD patterns and (b) FTIR spectra of g-C_3N_4 and g-C_3N_4@ZIF-8; (c) UV-visible spectra of g-C_3N_4 and g-C_3N_4@ZIF-8; (d) PL spectra of g-C_3N_4@ZIF-8 with excitation of different wavelengths.
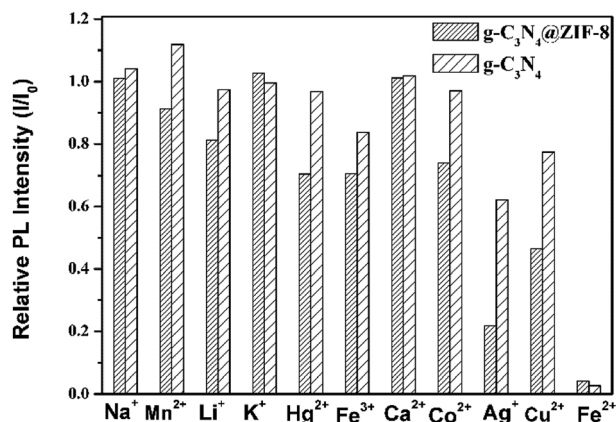
Fig. 4 Differences in PL intensities of g-C$_3$N$_4$ and g-C$_3$N$_4$@ZIF-8 between blank and solutions containing different metal ions (λ_{ex} = 330 nm, metal ion concentration of 66 ppm).

number of metal ions can interact with g-C$_3$N$_4$. Therefore, g-C$_3$N$_4$@ZIF-8 had a higher sensitivity than g-C$_3$N$_4$, especially for Ag$^+$ and Cu^{2+}. Additionally, using DMF replacing water could limit the hydrolysis of transition metal ions.

To evaluate the g-C$_3$N$_4$@ZIF-8 and g-C$_3$N$_4$'s sensitivities toward different concentrations of Cu^{2+}, Ag$^+$ and Fe^{2+}, PL intensities were monitored by the titration method. The enhanced selectivity was observed for Cu^{2+} and Ag$^+$. Therefore, these two ions were tested by g-C$_3$N$_4$@ZIF-8 and g-C$_3$N$_4$, individually. It can be seen from Fig. 5a and b that the PL intensity of g-C$_3$N$_4$@ZIF-8 and g-C$_3$N$_4$ decreased gradually with increasing of Cu^{2+} concentrations. The limit of detection (LOD) for sensing Cu^{2+} by g-C$_3$N$_4$@ZIF-8 was about 11.2 ppm because less Cu^{2+} did not influence the PL intensity. A linear relationship between Cu^{2+} concentration and PL intensity in the range of 5 ppm to 11 ppm was obtained (Fig. 5g). The LOD of Cu^{2+} was lower than the maximum allowable level of Cu^{2+} (~20 μM) in the drinking water regulated by US Environmental Protection Agency (EPA).[44] While for the g-C$_3$N$_4$, the LOD for sensing Cu^{2+} was about 22.8 ppm. It indicated that the using of g-C$_3$N$_4$@ZIF-8 for sensing Cu^{2+} was able to increase the LOD by about 100%. Similar to Cu^{2+}, with increasing in the concentrations of Ag$^+$, the PL intensities of g-C$_3$N$_4$@ZIF-8 and g-C$_3$N$_4$ gradually decreased (Fig. 5c and d). The LOD for sensing Ag$^+$ by g-C$_3$N$_4$@ZIF-8 and g-C$_3$N$_4$ was 13.2 ppm and 33.8 ppm, respectively. The LOD for sensing Ag$^+$ by g-C$_3$N$_4$@ZIF-8 was enhanced by about 250%. A linear response was also obtained for sensing Ag$^+$ by g-C$_3$N$_4$@ZIF-8 (Fig. 5h).

Organic dyes were the most commonly used sensing material to distinguish Fe^{2+} and Fe^{3+} due to its convenient and selectively.[45] However, organic dyes are only specific to one kind of metal ions, which can't be used for the detection of several kinds of metal ions. In this work, g-C$_3$N$_4$ nanosheet and g-C$_3$N$_4$@ZIF-8 can be easily prepared, which show the capability of sensing Fe^{2+} with high selectivity (Fig. 5e and f). It indicated that the LOD of Fe^{2+} by g-C$_3$N$_4$@ZIF-8 was about 65.4 ppm with a linear range of 0–30 ppm.
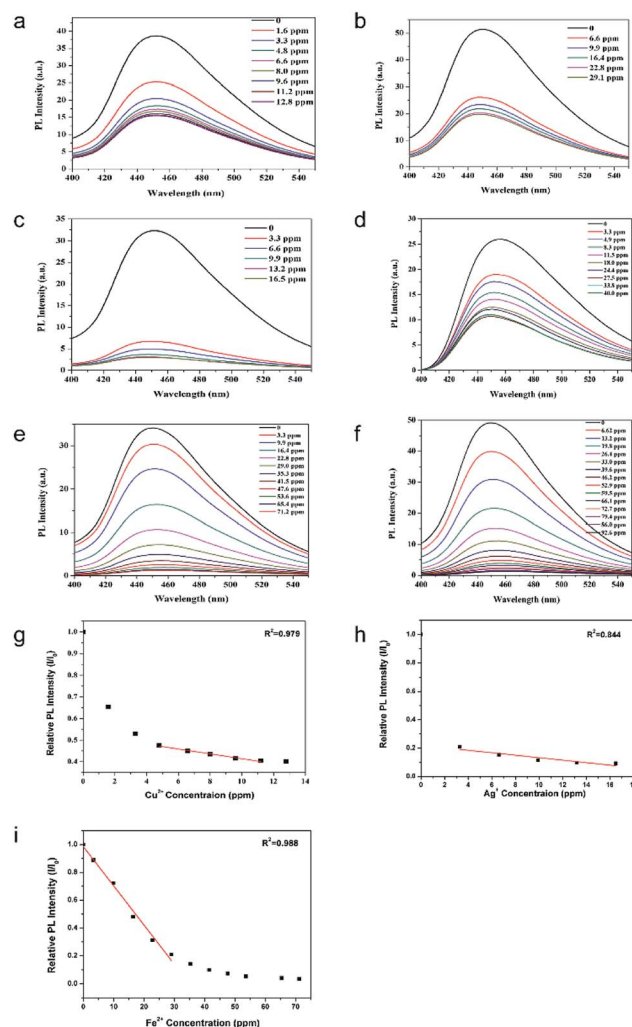

Fig. 5 (a) and (b) PL intensity evolution of (a) g-C$_3$N$_4$@ZIF-8 and (b) g-C$_3$N$_4$ in the presence of different concentrations of Cu^{2+}; (c) and (d) PL intensity evolution of (c) g-C$_3$N$_4$@ZIF-8 and (d) g-C$_3$N$_4$ in the presence of different concentrations of Ag$^+$; (e) and (f) PL intensity evolution of (c) g-C$_3$N$_4$@ZIF-8 and (d) g-C$_3$N$_4$ in the presence of different concentrations of Fe^{2+}; linear regression line of PL intensities of g-C$_3$N$_4$@ZIF-8 for sensing (g) Cu^{2+}, (h) Ag$^+$ and (i) Fe^{2+}. I and I_0 are PL intensities of in the presence and absence of metal ions, respectively.

3.3 Detection of specific solvents

Changes in the PL intensities of g-C$_3$N$_4$@ZIF-8 and g-C$_3$N$_4$ in different solvents were also investigated. Various solvents were tested as a comparison to the PL intensity of g-C$_3$N$_4$@ZIF-8 and g-C$_3$N$_4$ in DMF. The PL intensity of H$_2$O was same to the DMF, indicating the replace of DMF to H$_2$O for the further solvent sensor. As shown in Fig. 6a, the relative PL intensities of g-C$_3$N$_4$@ZIF-8 to g-C$_3$N$_4$ were higher in THF than that of in other solvents. This selectivity can be used for detecting THF solvent. As shown in Fig. 6b, when the THF concentration was increased, the intensity of g-C$_3$N$_4$@ZIF-8 was increased gradually. An fitting linear relationship between the THF fraction and PL intensities (THF volume fraction from 0–1.0) was found by this method as shown in Fig. 6c. All the results suggested that this method provide a novel approach for the detection of THF in water solution.
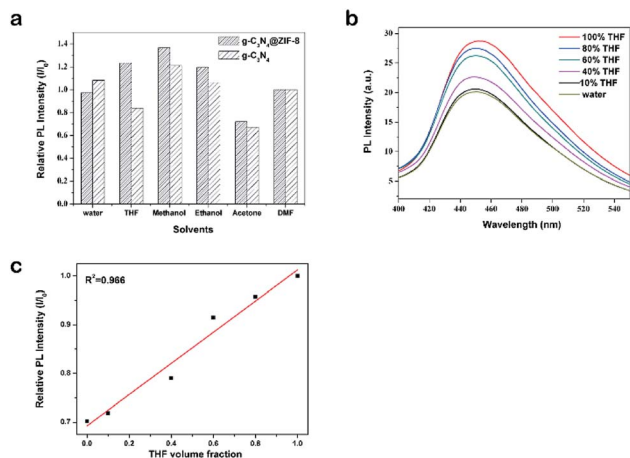
Fig. 6 (a) Relative PL intensities of g-C_3N_4 and g-C_3N_4@ZIF-8 in various solvents (λ_{ex} = 330 nm, particles concentration 60 ppm, I and I_0 are PL intensities of in the presence and absence of metal ions, respectively); (b) PL spectrum of different THF concentration in water (λ_{ex} = 330 nm); (c) linear regression line of relative intensities of g-C_3N_4@ZIF-8 with various THF volume fraction (λ_{em} = 450 nm).

4 Conclusions

In summary, g-C_3N_4@ZIF-8 nanocomposite was facial prepared, characterized and applied for the enhanced fluorescent detection of metal ions and solvents based on the PL measurement. The enhanced selectivity of g-C_3N_4@ZIF-8 to g-C_3N_4 was obvious in detecting Cu^{2+} and Ag^+. The sensitivities for the detection of Cu^{2+} and Ag^+ improve from 29.1 to 11.2 ppm and from 40 to 16.5 ppm, respectively. Comparing to Fe^{3+}, Fe^{2+} can selectively quench the fluorescence of g-C_3N_4@ZIF-8 and g-C_3N_4, which was successfully applied for distinguishing Fe^{3+} and Fe^{2+}. The LOD of Fe^{2+} by g-C_3N_4@ZIF-8 was as low as 65.4 ppm. The enhanced PL intensities of g-C_3N_4@ZIF-8 by the THF can be used for detecting THF in water with a good linear relationship (THF volume fraction from 0–1.0). With further development and optimization, it is expected that g-C_3N_4@ZIF-8 nanocomposite have great potential to be applied as fast and selective sensitive elements for enhanced fluorescence detection of metal ions and solvents.

Conflicts of interest

There are no conflicts to declare.

Acknowledgements

References

1 G. Aragay, J. Pons and A. Merkoçi, *Chem. Rev.*, 2011, **111**, 3433.

2 K. G. Daniel, R. H. Harbach, W. C. Guida and Q. P. Dou, *Front. Biosci.*, 2004, **9**, 2652.

3 H. T. Ratte, *Environ. Toxicol. Chem.*, 1999, **18**, 89.

4 L. Järup, *Br. Med. Bull.*, 2003, **68**, 167.

5 S. Su, B. Chen, M. He and B. Hu, *Talanta*, 2014, **123**, 1.

6 B. Dai, M. Cao, G. Fang, B. Liu, X. Dong, M. Pan and S. Wang, *J. Hazard. Mater.*, 2012, **219**, 103.

7 Y. X. Yuan, L. Ling, X. Y. Wang, M. Wang, R. A. Gu and J. L. Yao, *J. Raman Spectrosc.*, 2007, **38**, 1280.

8 G. Aragay, J. Pons and A. Merkoci, *J. Mater. Chem.*, 2011, **21**, 4326.

9 S. Goswami and R. Chakrabarty, *Tetrahedron Lett.*, 2009, **50**, 5910.

10 K. T. Yong, W. C. Law, R. Hu, L. Ye, L. Liu, M. T. Swihart and P. N. Prasad, *Chem. Soc. Rev.*, 2013, **42**, 1236.

11 H. C. Zhou, J. R. Long and O. M. Yaghi, *Chem. Rev.*, 2012, **112**, 673.

12 J. R. Li, J. Sculley and H. C. Zhou, *Chem. Rev.*, 2011, **112**, 869.

13 J. Lee, O. K. Farha, J. Roberts, K. A. Scheidt, S. T. Nguyen and J. T. Hupp, *Chem. Soc. Rev.*, 2009, **38**, 1450.

14 L. E. Kreno, K. Leong, O. K. Farha, M. Allendorf, R. P. Van Duyne and J. T. Hupp, *Chem. Rev.*, 2011, **112**, 1105.

15 P. Horcajada, R. Gref, T. Baati, P. K. Allan, G. Maurin, P. Couvreur, G. Férey, R. E. Morris and C. Serre, *Chem. Rev.*, 2011, **112**, 1232.

16 R. Banerjee, A. Phan, B. Wang, C. Knobler, H. Furukawa, M. O'Keeffe and O. M. Yaghi, *Science*, 2008, **319**, 939.

17 B. Chen, L. Wang, Y. Xiao, F. R. Fronczek, M. Xue, Y. Cui and G. Qian, *Angew. Chem., Int. Ed.*, 2009, **48**, 500.

18 A. Salinas-Castillo, M. Camprubi-Robles and R. Mallavia, *Chem. Commun.*, 2010, **46**, 1263.

19 S. Liu, Z. Xiang, Z. Hu, X. Zheng and D. Cao, *J. Mater. Chem.*, 2011, **21**, 6649.

20 T. T. Han, H. L. Bai, Y. Y. Liu and J. F. Ma, *J. Solid State Chem.*, 2019, **269**, 588.

21 J. Wang, H. Chen, F. Ru, Z. Zhang, X. Mao, D. Shan, J. Chen and X. Lu, *Chem.–Eur. J.*, 2018, **24**, 3449.

22 Y. Xu, S. Wu, X. Li, Z. Wang, Y. Han, J. Wu and X. Zhang, *Mater. Lett.*, 2018, **210**, 235.

23 F. Su, S. C. Mathew, G. Lipner, X. Fu, M. Antonietti, S. Blechert and X. Wang, *J. Am. Chem. Soc.*, 2010, **132**, 16299.

24 D. J. Martin, K. Qiu, S. A. Shevlin, A. D. Handoko, X. Chen, Z. Guo and J. Tang, *Angew. Chem., Int. Ed.*, 2014, **53**, 9240.

25 S. C. Yan, Z. S. Li and Z. G. Zou, *Langmuir*, 2010, **26**, 3894.

26 J. Tian, Q. Liu, A. M. Asiri, A. O. Al-Youbi and X. Sun, *Anal. Chem.*, 2013, **85**, 5595.

27 S. Barman and M. Sadhukhan, *J. Mater. Chem.*, 2012, **22**, 21832.

28 H. Huang, R. Chen, J. Ma, L. Yan, Y. Zhao, Y. Wang, W. Zhang, J. Fan and X. Chen, *Chem. Commun.*, 2014, **50**, 15415.

29 S. Zhang, J. Li, M. Zeng, J. Xu, X. Wang and W. Hu, *Nanoscale*, 2014, **6**, 4157.

30 Y. Gong, Y. Wang, G. Sun, T. Jia, L. Jia, F. Zhang, L. Lin, B. Zhang, J. Cao and Z. Zhang, *Nanomaterials*, 2018, **8**, 132.

31 S. Chen, N. Hao, D. Jiang, X. Zhang, Z. Zhou, Y. Zhang and K. Wang, *J. Electroanal. Chem.*, 2017, **787**, 66.

32 H. Li, M. Yang, J. Liu, Y. Zhang, Y. Yang, H. Huang, Y. Liu and Z. Kang, *Nanoscale*, 2015, **7**, 12068.

33 S. Ansari, M. S. Ansari, H. Devnai, S. P. Satsangee and R. Jain, *Sens. Actuators, B*, 2018, **273**, 1226.

34 C. Sun, M. Zhang, Q. Fei, D. Wang, Z. Sun, Z. Geng, W. Xu and F. Liu, *Sens. Actuators, B*, 2018, **256**, 160.

35 S. Hu, W. Quyang, L. Guo, Z. Lin, X. Jiang, B. Qiu and G. Chen, *Biosens. Bioelectron.*, 2017, **92**, 718.

36 S. Zhang, N. Hang, Z. Zhang, H. Yue and W. Yang, *Nanomaterials*, 2017, **7**, 12.

37 H. Wang, Z. Guo, W. Hao, L. Sun, Y. Zhang and E. Cao, *Mater. Lett.*, 2019, **234**, 40.

38 S. De, N. Venkataramani, S. Prasad, R. O. Dusane, L. Presmanes, Y. Thimont, P. Taihades, V. Baco-Carles, C. Bonningue, S. T. Pisharam and A. Barnabe, *IEEE Sens. J.*, 2018, **18**, 6937.

39 P. Niu, L. Zhang, G. Liu and H. M. Cheng, *Adv. Funct. Mater.*, 2012, **22**, 4763.

40 I. Pastoriza-Santos and L. M. Liz-Marzán, *Langmuir*, 1999, **15**, 948.

41 Y. Hu, H. Kazemian, S. Rohani, Y. Huang and Y. Song, *Chem. Commun.*, 2011, **47**, 12694.

42 Y. Zhang, S. Meng, J. Ding, Q. Peng and Y. Yu, *Analyst*, 2019, **144**, 504.

43 S. Lee, Y. Jun, E. Lee, N. Heo, W. Hong, Y. Huh and Y. Chang, *Carbon*, 2015, **95**, 58.

44 Y. T. Su, G. Y. Lan, W. Y. Chen and H. T. Chang, *Anal. Chem.*, 2010, **82**, 8566.

45 J. W. Stucki, *Soil Sci. Soc. Am. J.*, 1981, **45**, 638.